Modification of Indium Tin Oxide Films by Alkanethiol and Fatty Acid Self-Assembled Monolayers: A Comparative Study

ARTICLE *in* LANGMUIR · APRIL 2006

Impact Factor: 4.46 · DOI: 10.1021/la052677b · Source: PubMed

5 AUTHORS, INCLUDING:

P. Lang
French National Centre for Scientific Research
81 PUBLICATIONS **1,810** CITATIONS
SEE PROFILE

Mohamed Chehimi
Institut de Chimie et des Matériaux Paris-Est
269 PUBLICATIONS **5,443** CITATIONS
SEE PROFILE

Michel Delamar
Paris Diderot University
133 PUBLICATIONS **4,162** CITATIONS
SEE PROFILE

Gilles Horowitz
French National Centre for Scientific Research
240 PUBLICATIONS **11,350** CITATIONS
SEE PROFILE

Modification of Indium Tin Oxide Films by Alkanethiol and Fatty Acid Self-Assembled Monolayers: A Comparative Study

Nadia Karsi, Philippe Lang, Mohamed Chehimi, Michel Delamar, and Gilles Horowitz*

ITODYS, CNRS−UMR 7086, Université Denis-Diderot, 1 rue Guy de la Brosse, 75005 Paris, France

Received October 3, 2005. In Final Form: January 24, 2006

Indium tin oxide (ITO) substrates have been modified by alkanethiol and fatty acid self-assembled monolayers (SAMs). The SAMs were grown by dipping the cleaned surface into either a pure alkanethiol or a fatty acid dissolved in various solvents. They were characterized through contact angle, X-ray photoelectron (XPS) and infrared absorption−reflection spectroscopy (IRRAS). Their density and structural organization was found to greatly depend on the cleaning treatment of the ITO surface, the length of the alkyl chain, and, in the case of fatty acids, the concentration of the solution. XPS measurements brought evidence for the fact that, in the case of alkanethiols, the grafting mechanism was through the formation of ionic or covalent bonds involving thiolates. The most prominent result of this comparative study is that thiol-based SAMs are more strongly attached to the ITO substrate and better organized than fatty acids, which we attribute to the fact that the reaction of the ITO surface with fatty acids is more reversible than that with thiols.

Introduction

Because of its large availability, tin-doped indium oxide (ITO) has become the almost universal material for transparent electrodes in numerous applications. This is particularly true in devices in which organic materials are involved, such as liquid-crystal displays (LCDs), organic light-emitting diodes (OLEDs) and organic photovoltaic cells (OPVs). However, the manufacturing of ITO is widely variable, which leads to films that are very heterogeneous in chemical composition and electrical properties.[1−3] Moreover, these properties are very dependent on the physical and chemical surface treatment of the films.[1,2,4,5] For example, the work function of ITO films, a parameter of importance in the final performance of OLEDs and OPVs, may vary over several tenths of an electronvolt, depending on the surface preparation. Reported values range between 4 and 5 eV, which makes ITO a good candidate as an anode (hole injector) in organic diodes. However, it has been demonstrated that the interface between ITO and an organic semiconductor is far from following the simple Mott−Schottky model, which predicts that the hole injection barrier is given by the difference between the electrode work function and the energy of the highest occupied molecular orbital (HOMO).[6] Instead, an additional energy barrier forms at the interface that tends to shift the HOMO level downward, thus increasing the interface barrier by up to 1 eV. The origin of this shift is often attributed to some dipole moment resulting from the presence of unexpected localized charges at the interface.[7] A means to thwart the detrimental effect of these charges is to purposely graft on the surface of the electrode molecules bearing a counter-oriented dipole. Several works have been recently conducted with that in mind, in which the grafted molecule consists of a short conjugated core equipped with a donor group at one end and an acceptor group at the other end. The molecule is attached to the ITO surface through a reactive group that may also serve as a donor group. Because of this adsorption mechanism and the subsequent organization process, the thus formed monolayer is referred to as a self-assembled monolayer (SAM) that spontaneously comes out when dipping a substrate in a solution containing a molecule with a reactive functional element prone to bind to the surface. The nature of the reactive group is of primary importance for the quality, in terms of structure and density, of the SAM. To this respect, acids[8] and silanes[9,10] are the most often used reactive groups on ITO. However, a few recent reports have shown that thiols can also be considered for that purpose.[11−14]

This paper is devoted to a comparative study of the formation mechanism of SAMs made of fatty acid and alkanethiols. We show that the density and organization of the layer strongly depends on the preparation of the ITO substrate, on the length of the alkyl chain, and on the solvent and concentration of the solution used to prepare the monolayer. Surprisingly, thiols seem to lead to better-organized and denser layers.

Results

Preparation of the ITO Substrates. The contact angle, root-mean-square (rms) surface roughness, Kelvin-probe work function, and four-point sheet resistance of the as-received and treated ITO samples are summarized in Table 1. The surface treatment has a dramatic effect on contact angle, a slight but measurable effect on the work function, and practically no effect on the sheet

* Corresponding author. E-mail address: horowitz@paris7.jussieu.fr.

(1) Kim, J. S.; Granström, M.; Friend, R. H.; Johansson, N.; Salaneck, W. R.; Daik, R.; Feast, W. J.; Cacialli, F. *J. Appl. Phys.* **1998**, *84*, 6859.
(2) Kim, H.; Gilmore, C. M.; Horwitz, J. S.; Pique, A.; Murata, H.; Kushto, G. P.; Schlaf, R.; Kafafi, Z. H.; Chrisey, D. B. *Appl. Phys. Lett.* **2000**, *76*, 259.
(3) Donley, C.; Dunphy, D.; Paine, D.; Carter, C.; Nebesny, K.; Lee, P.; Alloway, D.; Armstrong, N. R. *Langmuir* **2002**, *18*, 450.
(4) Wu, C. C.; Wu, C. I.; Sturm, J. C.; Kahn, A. *Appl. Phys. Lett.* **1997**, *70*, 1348.
(5) Milliron, D. J.; Hill, I. G.; Shen, C.; Kahn, A.; Schwartz, J. *J. Appl. Phys.* **2000**, *87*, 572.
(6) Koch, N.; Kahn, A.; Ghijsen, J.; Pireaux, J.-J.; Schwartz, J.; Johnson, R. L.; Elschner, A. *Appl. Surf. Sci.* **2003**, *82*, 70.
(7) Ishii, H.; Sugiyama, K.; Ito, E.; Seki, K. *Adv. Mater.* **1999**, *11*, 605.
(8) Appelhans, D.; Ferse, D.; Adler, H. J. P.; Plieth, W.; Fikus, A.; Grundke, K.; Schmitt, F. J.; Bayer, T.; Adolphi, B. *Colloids Surf., A* **2000**, *161*, 203.
(9) Malinsky, J. E.; Jabbour, G. E.; Shaheen, S. E.; Anderson, J. D.; Richter, A. G.; Marks, T. J.; Armstrong, N. R.; Kippelen, B.; Dutta, P.; Peyghambarian, N. *Adv. Mater.* **1999**, *11*, 227.
(10) Lee, J.; Jung, B. J.; Lee, J. I.; Chu, H. Y.; Do, L. M.; Shim, H. K. *J. Mater. Chem.* **2002**, *12*, 3494.
(11) Kondo, T.; Takechi, M.; Sato, Y.; Uosaki, K. *J. Electroanal. Chem.* **1995**, *381*, 203.
(12) Yan, C.; Zharnikov, M.; Goelzhaeuser, A.; Grunze, M. *Langmuir* **2000**, *16*, 6208.
(13) Brewer, S. H.; Brown, D. A.; Franzen, S. *Langmuir* **2002**, *18*, 6857.
(14) Swint, A. L.; Bohn, P. W. *Langmuir* **2004**, *20*, 4076.

10.1021/la052677b CCC: $33.50
Published on Web 02/25/2006

Table 1. Surface Preparation of the ITO Films and Resulting Physical Parameters

#	surface treatment	contact angle (°)	rms[a] roughness (nm)	work function (eV)	sheet resistance (±2 Ω/□)	Sn/In[b] before[c]	Sn/In[b] after[c]	O/(In+Sn)[b] before[c]	O/(In+Sn)[b] after[c]	O_{hydrox}/O_{total} [b] before[c]	O_{hydrox}/O_{total} [b] after[c]
0	as received	97	0.90	4.50	41	0.12	N/A	0.33	N/A	0.29	N/A
1	UV−ozone	6−10	1.80	4.75	40	0.12	0.11	0.26	0.20	0.20	0.04
2	UV+H_2SO_4	10	1.90	4.65	40	0.12	0.12	0.25	0.21	0.14	0.05
3	UV+NaOH	8	1.78	4.59	37	0.12	0.11	0.25	0.20	0.11	0.04
4	UV+NaOH+H_2SO_4	< 5	1.78	4.55	39	0.12	0.12	0.23	0.22	0.09	0.05
5	Son[d]+NaOH+H_2SO_4	< 5	1.24	4.45	38	0.12	0.11	0.24	0.21	0.09	0.05

[a] rms: root-mean-square. [b] Integrated XPS signal ratio. [c] Before and after in situ ion etching in the XPS chamber. [d] Son: sonication in ultrapure water.

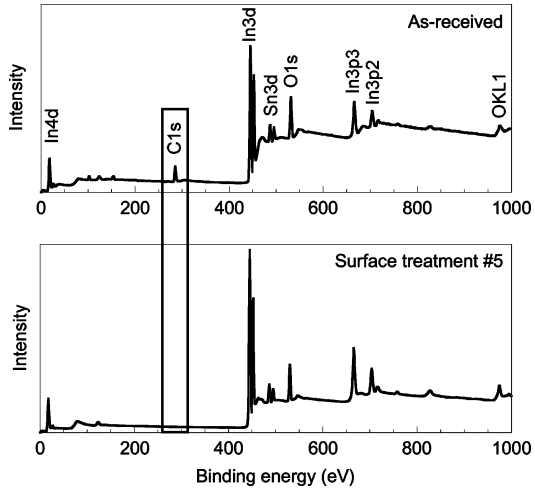

Figure 1. Survey XPS spectra of as-received (top) and cleaned (bottom) ITO films.

resistance. These results can be compared to those reported elsewhere.[1] We note that the UV−ozone treatment tends to increase the work function, while NaOH has the reverse effect. We also note that the roughness increases after cleaning, particularly when a UV−ozone treatment is involved in the process.

The survey X-ray photoelectron spectroscopy (XPS) spectra of the as-received samples and those cleaned with treatment #5 are shown in Figure 1. As expected, we detect oxygen, tin, and indium. Note that the most prominent difference between the two spectra is the carbon that is only present in the as-received sample. The origin of the carbon, and more specifically the hydrocarbons, can therefore be ascribed to surface contamination.

The high-resolution spectra for O1*s*, In3$d_{5/2}$, Sn3$d_{5/2}$, and C1*s* of the as-received substrate are displayed in Figure 2. The O1*s* signal could be decomposed into four peaks labeled A (530.4 eV), B (531.5 eV), C (532.5 eV), and D (533.5 eV). Peak C is attributed to hydroxyl groups,[3] while peak D corresponds to CO_3^{2-} and CO_2^- groups and is thus related to surface contamination. There is some controversy in the attribution of peaks A and B. Some studies have attributed these components to oxygen bound to indium and tin, respectively.[12] This appears to be unlikely because the ratio of the areas of the peaks is too far from that between indium and tin (see below). As pointed out by Fan and Goodenough,[15] such a double peak is typical for oxides of multiple valence cations. It has therefore been suggested that the O_2^- ions in peak A are surrounded by In atoms with their full complement of six O_2^- ions, while peak B corresponds to O_2^- ions located close to an oxygen vacancy. The In and Sn signals are not affected by these oxygen vacancies because oxygen ions give part of their electronic density to In and Sn. In turn, this electron density transfer leads to the shift of the O1*s* toward higher binding energy.

The signals for In and Sn are each made of two peaks, peaks E (444.5 eV) and F (445.5 eV) for In, and peaks H (486.6 eV) and I (486.6 eV) for Sn. The peaks E and H are attributed to the oxide, and peaks F and I are attributed to the hydroxide.[3,12] A weak peak G (446.5 eV) was added to improve the fitting of the In signal. It may arise from contamination or final state effects in the photoemission process.

Table 1 also gives various ratios between the integrated XPS signal of the constituents of the ITO films. The data can be compared to expected values estimated from the atomic composition of the ITO and the sensitivity of each element, as given by the manufacturer. Taking a sensitivity of 1 for C1*s*, the sensitivity is 2.93 for O1*s*, 13.32 for In3$d_{5/2}$, and 14.8 for Sn3$d_{5/2}$. The mean experimental ratio, Sn/In, is 0.115 ± 0.01, which is reasonably close to the expected 0.09 for an atomic ratio of 10%, as given by the supplier. Note that this ratio is hardly affected when neglecting peak G in the In3$d_{5/2}$ signal. As for the ratio O/(In+Sn), its expected value for a mean bulk composition, $(In_2O_3)_{0.9}(SnO_2)_{0.1}$, is 0.33. The measured numbers are all smaller than this expected value, except for the as-received sample. Because XPS only detects atoms localized at the surface, this discrepancy can be ascribed to the fact that the crystal planes at the surface are those rich in indium and tin. The higher value found before cleaning is likely due to contamination. Also indicated in Table 1 is the ratio of hydroxyl groups (peak C in Figure 2) to the total amount of oxygen. Again, the numbers dramatically decrease after etching, indicating that most of the hydroxides comes from surface contamination. After cleaning and etching, the amount of hydroxide falls to around 5%, whichever surface treatment is used.

Alkanethiol SAMs on ITO. Alkanethiol SAMs were grown by dipping ITO substrates in pure decanethiol (SHC_{10}), dodecanethiol (SHC_{12}), or octadecanethiol (SHC_{18}).

Contact Angle. The adsorption kinetics was followed by measuring at each step the static contact angle. The data obtained on substrates prepared with surface treatment #5 are illustrated in Figure 3. For SHC_{10} and SHC_{12}, the angle increases rapidly between 5 and 30 min, and more slowly up to 16 h, where it stabilizes to its maximum value. The kinetics is much faster with SHC_{18}, where the angle already saturates after 5 min. In all three cases, the maximum angle (110 ± 2°) is practically the same.

IR Absorption. Figure 4 shows the infrared absorption at normal incidence of alkanethiol SAMs in the region of the $\nu(CH_2)$ and $\nu(CH_3)$ vibration modes for various alkyl chain lengths (top panel) and surface treatments of the ITO substrate (bottom panel). The frequency and full width at half-maximum (fwhm) of the peaks are gathered in Table 2. The intensity of the peaks increases with the length of the alkyl chain, and, for SCH_{18}, it increases when passing from treatment #1 to treatment #5. As will be discussed later, higher intensity may come from several

(15) Fan, J. C. C.; Goodenough, J. B. *J. Appl. Phys.* **1977**, *48*, 3524.

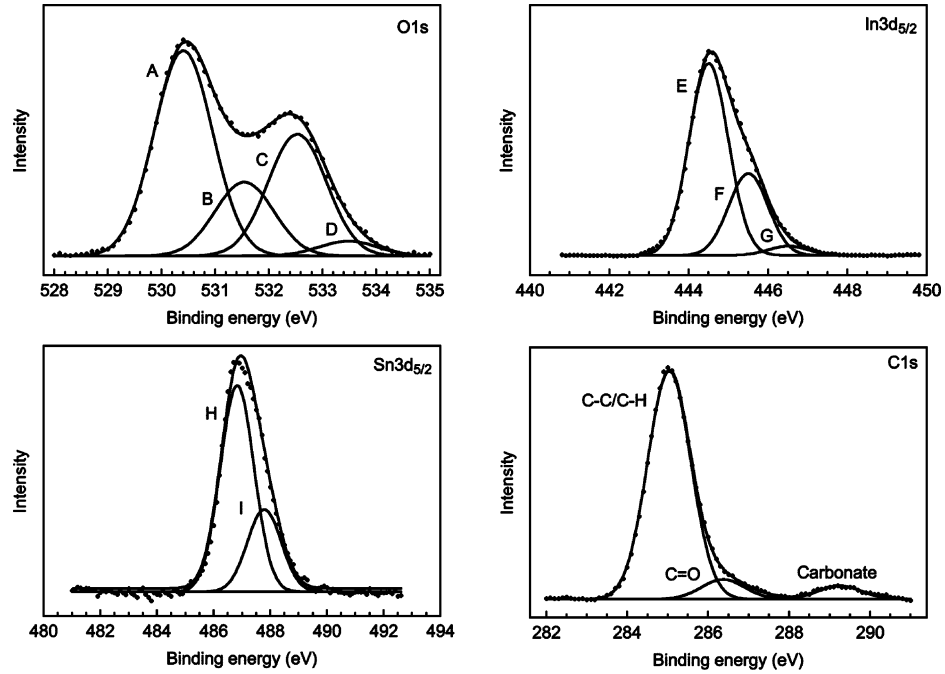

Figure 2. High-resolution XPS spectra of O1*s*, In3$d_{5/2}$, Sn3$d_{5/2}$, and C1*s* recorded on an as-received ITO film.

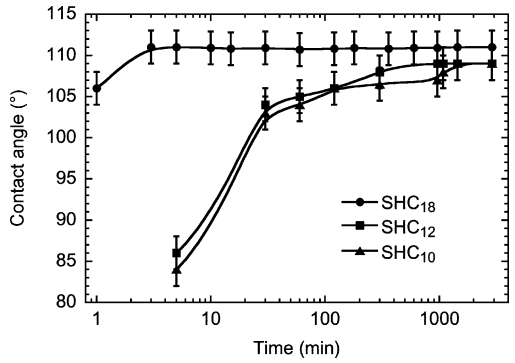

Figure 3. Variation of the contact angle with adsorption time for alkanethiol SAMs with three different chain lengths.

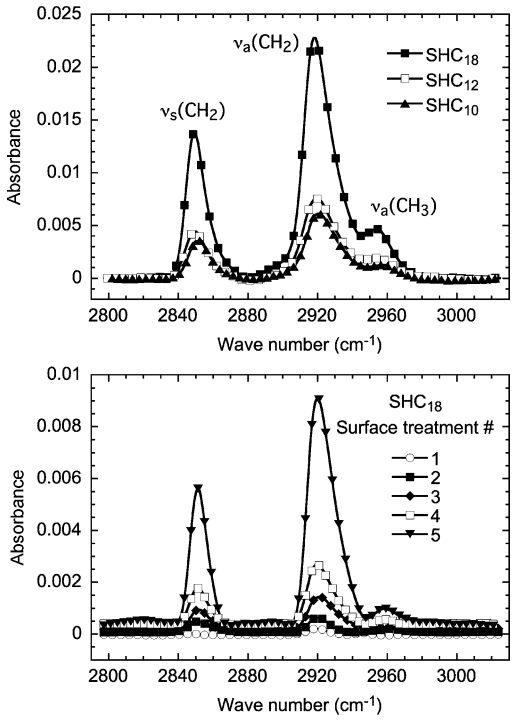

Figure 4. Normal incidence IR absorption of alkanethiol SAMs on ITO for various lengths of the alkyl chain (top) and various treatments of the ITO substrate (bottom). Surface treatments are detailed in Table 1.

factors. Thicker films and higher coverage are the more obvious explanations. However, because, at normal incidence, the IR light is polarized parallel to the ITO surface, another possible origin is a change in the average tilt angle of the alkyl chains.

It is worth pointing out at this stage that the resolution of IR measurements corresponds to the minimum distance between two peaks for the peaks to be resolved. However, the accuracy in the position of a given band is more a problem of signal-to-noise ratio; it is most often better than the resolution, and was estimated to be 1 cm^{-1} in our case.

The frequency of the $\nu_a(CH_2)$ mode is indicative of the conformation of the alkyl chain. As can be seen in the two last lines in Table 2, the frequency changes from 2918 cm^{-1} in solid SHC_{18}, where most of the alkyl chains are in all-trans conformation, to 2927 cm^{-1} in liquid SHC_{18}, which contains gauche chains. A mean value of 2920 cm^{-1} is observed on our SAMs, thus indicating a low amount of gauche defects. Focusing on the SAMs with a dipping time of 16 h (the first three lines), we note that the longer the alkyl chain, the closer the frequency is to that of the solid state, thus indicating that full self-assembly is only achieved when $n > 12$, where n is the number of carbon atoms in the alkyl chain.

The infrared data were used to estimate the average tilt angle of the alkyl chains. The calculation rests on a judicious choice of absorption modes with differently oriented transition dipoles. The set of coordinates used to establish the orientation of the molecule is depicted in Figure 5. α is the tilt angle of the long axis with respect to the normal to the surface, and β corresponds to the rotation of the plane of the carbon backbone with respect to the plane defined by the normal to the substrate and the long axis of the molecule. At normal incidence, the electric field of the IR wave is parallel to the substrate, and only the projection of the transition moment of the vibration modes on this plane has to be taken into account. The calculation is developed in the

Table 2. Frequency and fwhm of the $\nu(CH_2)$ and $\nu(CH_3)$ Peaks in Figure 4

SAM (time)	ITO treatment #	$\nu_s(CH_2)$ σ (cm^{-1})	$\nu_s(CH_2)$ fwhm	$\nu_a(CH_2)$ σ (cm^{-1})	$\nu_a(CH_2)$ fwhm	$\nu_a(CH_3)$ σ (cm^{-1})	$\nu_a(CH_3)$ fwhm
SHC_{10} (16 h)		2851	16	2920	18	2957	10
SHC_{12} (16 h)	5	2850	16	2919	19	2955	19
SHC_{18} (16 h)		2849	14	2818	19	2954	9
	1	2847	11	2920	16	2958	20
	2	2851	15	2920	15	2962	14
SHC_{18} (5 min)	3	2852	13	2921	19	2958	10
	4	2851	12	2920	19	2957	11
	5	2852	15	2920	17	2955	9
solid SHC_{18}		2855	8−12	2918	8−12	2957	8−12
liquid SHC_{18}		2851	14	2927	23	2959	17

Supporting Information. To estimate the tilt angle α, we made use of the $\nu_a(CH_3)$ and $\nu_s(CH_2)$ modes. With only two modes, an independent determination of the rotation angle β was not possible. We made the assumption that $\beta = 45°$, which will be justified later. The results are gathered in Table 3.

XPS. The nature of the chemical bonding involved in the formation of the SAMs was elucidated through XPS measurements. The top panel of Figure 6 shows the high-resolution XPS spectrum of sulfur S2*p* for a SHC_{18} SAM. The signal can be decomposed into two components. The first one is made of a peak at 162.0 eV and its doublet at 163.2 eV with an intensity ratio of 2:1; it corresponds to a thiolate, and indicates the formation of an ionic or covalent bonding of sulfur with In or Sn, or both. The second component is more complex; it comprises several peaks ranging between 166 and 168 eV. The complexity of this second signal shows that it probably originates from several species, among which we may suspect oxidized sulfur (SO_2^-) and disulfide (S−S). The origin of this second signal is not clear, but we believe it comes from thiols that did not react with the substrate and have been oxidized by the X-ray irradiation during the measuring process. The thiol head of these molecules is likely to be located at the surface of the SAM. Evidence for such statements comes from the fact that (1) the magnitude of the signal increases with the irradiation time, and (2) the signal is substantially reduced after a short ion etch of the samples, which

Table 3. Average Tilt Angle α and Rotation Angle β of the Molecules in SAMs

substrate	treatment #	SAM (adsorp. time)	concentration (M/L)	α (°)	β (°)
ITO[a]	1		pure	51 ± 5	45[c]
	2			47 ± 5	
	3	SHC_{18} (5 min)		48 ± 5	
	4			39 ± 5	
	5			34 ± 5	
		SHC_{10} (16 h)		47 ± 5	
	5	SHC_{12} (16 h)		39 ± 5	
		SHC_{18} (16 h)		34 ± 5	
InO_x[b]		SHC_{18} (16 h)	pure	36 ± 2	43 ± 2
SnO_x[b]				35 ± 2	42 ± 2
ITO[a]	5	eicosanoic acid (1 h)	5×10^{-4}	34 ± 5	45[c]
			10^{-3}	49 ± 5	
			10^{-2}	53 ± 5	

[a] From the IR absorption at normal incidence. [b] From PMIRRAS. [c] A rotation angle of 45° is assumed in this case.

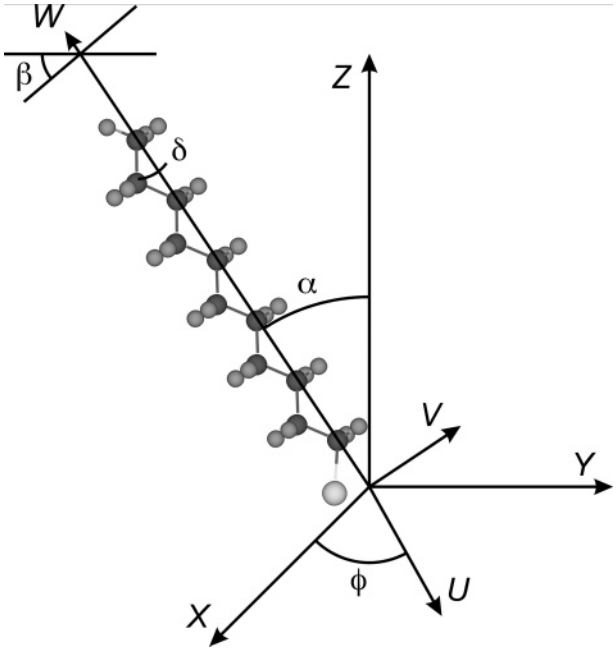

Figure 5. The system of coordinates used for the calculation of the orientation of the alkanethiol molecule. Axes *X*, *Y*, and *Z* refer to the substrate, and *U*, *V*, and *W* refer to the molecule. α is the angle between the molecule's long axis and the normal to the surface, and β is the rotation of the plane of the carbon backbone with respect to the plane defined by the normal to the surface and the molecule's long axis.

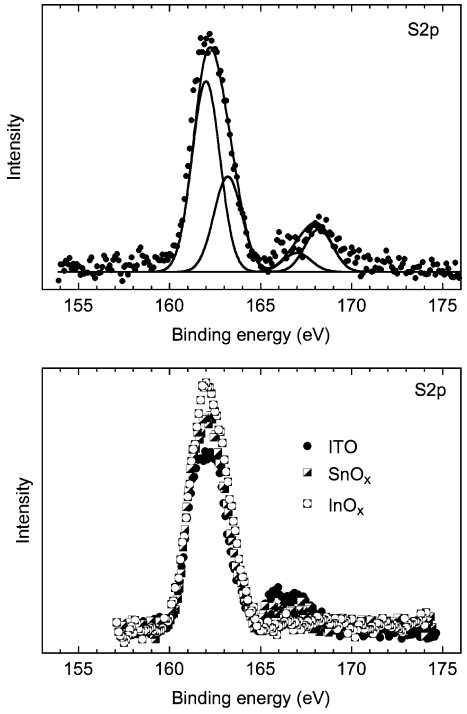

Figure 6. High-resolution XPS S2*p* signal of SHC_{18} SAMs on ITO (top) and ITO and oxidized Sn and In (bottom).

Table 4. Ratio of the Integrated XPS Signal of Sulfur to the Sum of that of Indium and Tin for the Various Cleaning Processes of the ITO Substrate

treatment #	1	2	3	4	5
S/(In+Sn)	0.25	0.28	0.38	0.50	0.81

shows that the species associated with the signal are located at the extreme surface of the SAM rather than at the SAM−ITO interface.

Table 4 shows the evolution of the ratio of the integrated signal of sulfur to the sum of that of indium and tin as a function of the pretreatment of the ITO. These numbers can be taken as a rough estimation for the coverage of the ITO by the SAM. The coverage strongly depends on the cleaning treatment of the ITO, and reaches its maximum with treatment #5. Note that this result is at least qualitatively in good agreement with the respective intensity of the IR signal (see Figure 4).

Alkanethiols on Oxidized In and Sn. Oxidized indium and tin substrates were prepared by vapor-depositing 100 nm thick films of the pure metal on a glass substrate and allowing them to oxidize in air. Because, in these cases, the substrate is a metal, the technique of surface polarization-modulated infrared reflection−absorption spectroscopy (PMIRRAS) could be used. Representative spectra are shown in Figure 7. Note that the intensity is given in relative units because the magnitude of the PMIRRAS signal is very sensitive to the position of the sample, and cannot be reliably compared from one sample to the other.

Comparing the frequency and fwhm of the PMIRRAS modes of the SAMs with those of the solid and liquid phases (Table 5), it can be stated that, in both cases, the SAMs are well organized and the amount of gauche defects is weak, thus indicating that the SAMs can be grafted on both substrates.

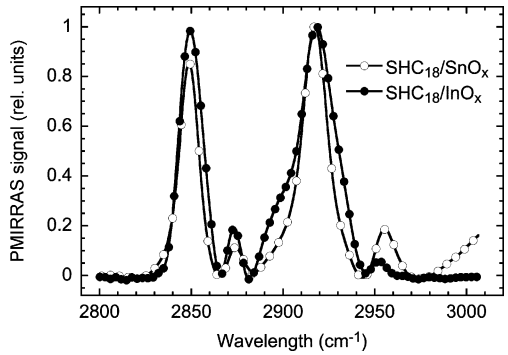

Figure 7. PMIRRAS spectra of SCH_{18} SAMs (adsorption time: 16 h) on oxidized Sn and In.

The bottom panel of Figure 6 compares the S2*p* high-resolution peak on oxidized In and Sn with that on ITO. We note that, while the ITO substrate was cleaned with treatment #5, which includes etching with H_2SO_4 and NaOH, the preparation of oxidized In and Sn only involved a UV−ozone treatment because both oxides tend to dissolve in acids and bases. The corresponding S/(In + Sn) ratio is 1.25 for oxidized In and 1.3 for oxidized Sn, but only 0.85 for ITO. The first two numbers indicate practically equal coverage on In and Sn oxide, so it can be stated that thiols similarly adsorb on both oxides. As for the lower coverage on ITO, it probably arises from the fact that the roughness of ITO is 5−10 times higher than that of the oxidized In and Sn films. The latter statement may also account for the fact that ITO is more difficult to clean.

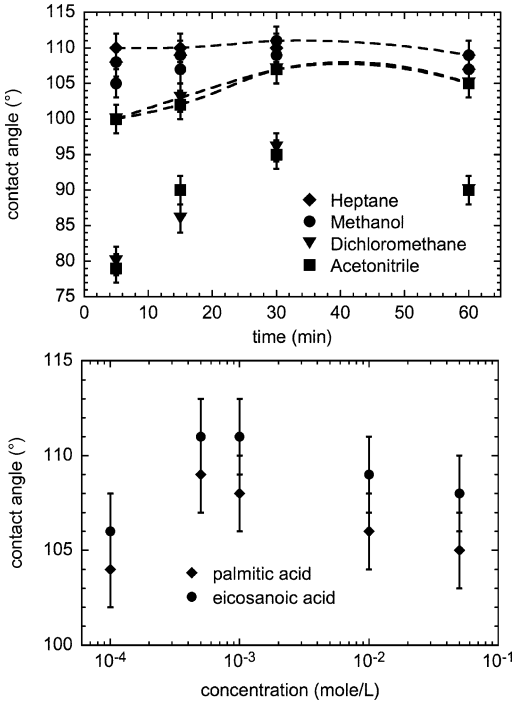

Figure 8. Top panel: Contact angle of eicosanoic acid SAMs as a function of adsorption time for various solvents. The concentration of the acid is 5×10^{-4} M/L. Data after thermal treatment (1 h at 80 °C) are indicated by dotted lines. Bottom panel: Contact angle of eicosanoic and palmitic acid SAMs as a function of the concentration of the solution. In both cases, the solvent is heptane.

As shown in the Supporting Information, the PMIRRAS data allow an independent estimation of the torsion and tilting angle of the molecule. The results are gathered in Table 3. We note that, in both cases, the rotation angle is close to 45°, which justifies the arbitrary choice made earlier in the case of ITO.

Fatty Acid SAMs on ITO. The acids used are palmitic acid ($CH_3(CH_2)_{14}COOH$) and eicosanoic acid ($CH_3(CH_2)_{18}COOH$).

Contact Angle. The top panel of Figure 8 shows the variation with the adsorption time of the contact angle of eicosanoic acid layers grown in various solvents. Also shown is the effect of a thermal treatment of the layers (1 h at 80 °C). In all cases, the contact angle increases with time up to 30 min, and then decreases. This is attributed to the formation of multilayers, as will be discussed later. The effect of thermal annealing is to improve the quality of the layer, particularly with dichloromethane and acetonitrile. The highest contact angles are obtained with heptane.

The variation of the contact angle with the concentration of the solution (in heptane) is shown in the bottom panel of Figure 8. In both cases, the angle reaches an optimum around 5×10^{-4} M/L. As stated above, we attribute the decrease in contact angle at higher concentration to the formation of multilayers.

Table 5. Frequency and fwhm of the PMIRRAS Modes of Alkanethiol SAMs on In and Sn Oxides

	$\nu_s(CH_2)$		$\nu_a(CH_2)$		$\nu_s(CH_3)$		$\nu_a(CH_3)$	
substrate	σ (cm^{-1})	fwhm	σ (cm^{-1})	fwhm	σ (cm^{-1})	fwhm	σ (cm^{-1})	fwhm
InO_x	2849	18	2918	24	2873	8	2952	7
SnO_x	2849	13	2917	16	2874	10	2955	10
solid SHC_{18}	2851	8−12	2918	8−12	2872	8−12	2957	8−12
liquid SHC_{18}	2855	14	2927	23	2873	9	2959	17

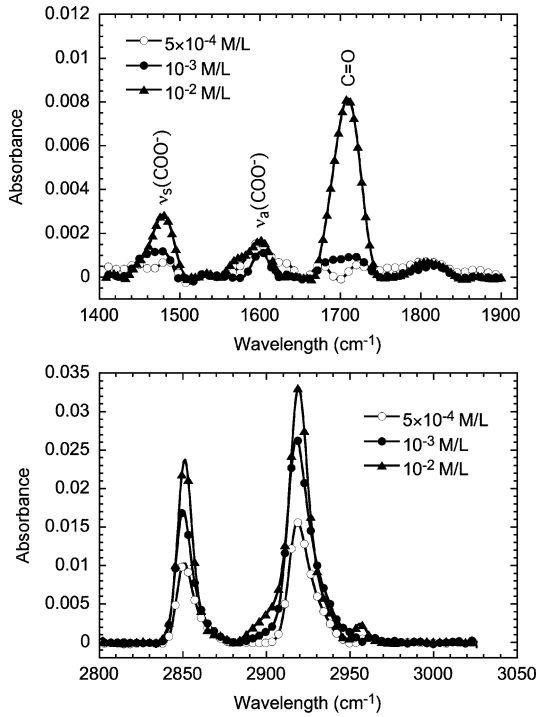

Figure 9. Normal incidence IR absorption spectra of eicosanoic acid SAMs for various concentrations of the solution (adsorption time: 1 h) in the 2800−3000 (bottom) and 1400−1900 cm^{-1} (top) domains.

Table 6. Frequency and fwhm of the IR Modes of Eicosanoic Acid SAMs on ITO

concentration	$\nu_s(CH_2)$		$\nu_a(CH_2)$		$\nu_a(CH_3)$	
(M/L)	σ (cm^{-1})	fwhm	σ (cm^{-1})	fwhm	σ (cm^{-1})	fwhm
5×10^{-4}	2848	15	2917	17	2957	12
10^{-3}	2850	15	2917	17	2957	12
10^{-2}	2849	13	2918	15	2954	10
solid	2849	9	2917	12	2954	5
liquid	2854	20	2924	27	2960	15

IR Absorption. Figure 9 shows the IR absorption of eicosanoic acid SAMs. The peak frequencies are gathered in Table 6. We note that, in all cases, the frequency of the $\nu_a(CH_2)$ mode is close to the value in the solid, which indicates that the molecules are mostly in all-trans configuration.

The peaks at 1479 and 1602 cm^{-1} (top panel of Figure 9) are attributed to the symmetric and antisymmetric COO^- stretching modes. The peak around 1700 cm^{-1} is assigned to the carbonyl C═O stretch for the H-bonded dimer.[16] Its growth at high concentrations is indicative of the formation of multilayers.

The average tilt angle of the molecules with respect to the normal to the ITO substrate was estimated, as done previously, from the IR data; the results are given in Table 3. Interestingly, the tilt angle increases with the concentration of the adsorption solution, which provides additional evidence for the formation of multilayers in films produced in highly concentrated solutions.

Discussion

The purpose of this section is to compare the respective anchoring strengths and levels of structural organization of alkanethiol and fatty acid films.

The anchoring strength was estimated by sonicating (i.e., rinsing in a ultrasonic cleaner) the SAM and measuring the contact angle. While thiol-based SAMs could be, in all cases, successfully ultrasonically rinsed after preparation without any change in contact angle, this was not the case with the fatty acid SAMs, which tended to peel off, as evidenced by an abrupt decrease in the contact angle. We note that this result does not go against that found by Yan and co-workers,[12] who observed that fatty acids preferentially adsorb over thiols when both are present in the solution. In short, the result by Yan comes from kinetics, while ours is more a question of thermodynamics. It may well be conceived that with the adsorption of fatty acids being more reversible (see below), their adsorption would be faster and their desorption would be easier.

The poor adhesion of fatty acids could also, at least in part, account for the tendency of fatty acids to form multilayers. For the time being, the reactions involved in the adsorption of thiols and fatty acids on ITO are not fully elucidated. We propose the following mechanisms. The adsorption of thiols would occur through the reaction R−SH + M → R−SM + H, where M is a metal atom. The reverse reaction, that is, desorption, would require the presence of a hydrogen atom, which is unlikely unless desorption takes place immediately after adsorption. So desorption requires the formation of a disulfide, RS−SR, with a Gibbs free energy close to 22 kcal/mol.[17] On the other hand, the energy to desorb a carboxylic acid is only 17 kcal/mol.[18] Again, the poorer resistance of fatty acids to peeling off would stem from a higher reversibility of the corresponding adsorption−desorption reaction.

An alternative origin of the higher anchoring strength of thiols is their better structural organization (see below). The reduced organization and density of acid SAMs might let water through the film, which, in turn, would favor desorption of the molecules. Evidence for better organization in thiols is brought by contact angle data. In all cases, the contact angle of thiols tends to saturate at longer adsorption times, while we observe a decrease with fatty acids. The latter is attributed to the formation of multilayers, as shown by the huge increase in the IR peak at 1704 cm^{-1} attributed to H-bounded dimers. However, we note that the average tilt angle is close to 35° for both well-organized thiols and fatty acid SAMs.

Conclusion

SAMs of alkanethiols and fatty acids have been successfully prepared on ITO substrate. The cleaning of the substrate is crucial for obtaining dense and well-organized films. The best results included etching with both acid and base, while the UV−ozone process did not appear to be indispensable. The reaction responsible for the chemisorption of thiols involves the formation of thiolates. Well-behaved SAMs could be grown on both oxidized indium and tin, and XPS measurements show that the binding reaction can take place with both metals. Sonication tests coupled to contact angle measurements showed that alkanethiols are more strongly bound to ITO than fatty acids. Further evidence for that is brought by the fact that multilayers tend to form with fatty acids for long dipping times or concentrated solutions. The origin of this difference is tentatively attributed to a higher reversibility of the adsorption−desorption reaction with fatty acids.

Experimental Section

Materials and Sample Preparation. ITO substrates were purchased from SOLEMS (Palaiseau, France). The average specification of the as-received ITO films is given in Table 1, and a

(16) Socrates, G. *Infrared Characteristic Group Frequencies: Tables and Charts*; John Wiley: New York, 1994.

(17) Karpovich, D. S.; Schessler, H. M.; Blanchard, G. J., The kinetics and thermodynamics of monolayer formation: In situ measurements of alkanethiol adsorption onto gold. In *Thin Films*; Ulman, A., Ed.; Academic Press: New York, 1997; Vol. 24, p 43.

(18) Ulman, A. *An Introduction to Ultrathin Organic Films*; Academic Press: New York, 1991.

detailed description of the preparation of the substrates can be found in the Results section.

All the vessels were carefully cleaned by boiling in pure sulfuric acid. Ultrapure water used for solutions and rinsing was taken directly from the water purification system (Elga UH2, 18 MΩ.cm).

The aliphatic thiols and acids (Aldrich) were used as received. The solvent was distilled under argon and put in contact with alumina balls (Merck) for at least 6 h. The alumina balls were activated by heating in an oven (400 °C) for several hours. NaOH solutions (8 M) were prepared from pellets (Merck Normapur). Sulfuric acid (98% suprapur) was purchased from Aldrich.

Sonication was performed in pure water with a Type T-460H Bioblock-Scientific ultrasonic bath at a frequency of 35 kHz and a power of 35 W.

Analytical Methods. Static contact angles were measured with a Digidrop GBX set up equipped with a CCD camera and analysis software under water-saturated ambient conditions.

The work function was estimated using a Kelvin probe (Monroe) installed inside a glovebox.

Sheet resistance was measured by the four-probe technique with a Keithley 2400 source-measurement unit.

IR spectra were recorded with a Nicolet 860 Fourier transform infrared (FTIR) (Thermo Electron) spectrometer with a resolution of 8 cm^{-1} by adding 2000 scans with an optical mirror velocity of 0.474 cm^{-1}/s. The resolution was chosen to increase the signal-to-noise ratio. Normal incidence spectra were obtained by growing the SAMs on ITO films deposited on highly resistive silicon wafers and were corrected for the absorption of the substrate. For PMIRRAS, the spectrometer was equipped with a commercially available module (Thermo Electron) including a ZnSe photoelastic modulator (PEM). PMIRRAS measurements were performed at an incident angle of 80°. After reflecting on the sample, the incident beam was focused with a ZnSe lens ($f = 5$m) on a MCT-A detector cooled to 77 K. The PEM oscillates at a frequency of 50 kHz and changes the polarization of the incident beam from parallel to perpendicular to the plane of incidence at a frequency of 100 kHz. The polarization-modulated signal is separated from the low frequency signal (between 380 and 3800 Hz) with a 48 kHz high-pass filter (GWC) and then demodulated. The two interferograms are high-pass and low-pass filtered by the spectrometer and simultaneously sampled by dual-channel electronics. Note that the PMIRRAS technique does not require any correction for the absorption of the substrate.

XPS signals were recorded using a VG Scientific ESCALAB 250 system equipped with a microfocused, monochromatic Al Kα X-ray source (1486.6 eV) and a magnetic lens that increases the electron acceptance angle and hence the sensitivity. A 650 μm X-ray beam was used at 20 mA × 15 kV. The samples were pressed against double-sided adhesive tape mounted on the sample holders. The spectra were acquired in the constant analyzer energy mode, with pass energies of 150 and 40 eV for the survey and narrow regions, respectively. In addition, ultimate spectral resolution was achieved for the C1*s* and S2*p* regions by setting the pass energy at 10 eV. Charge compensation was achieved with an electron flood gun combined with an argon ion gun. The argon partial pressure was 2×10^{-8} mbar in the analysis chamber. Implanted argon was not detected at the surface of the materials under these conditions. With the combination of both electron and argon guns, the surface charge was negative but perfectly uniform. Avantage software version 1.85 (Thermo Electron) was used for digital acquisition and data processing. Spectra were calibrated by setting the C1*s* C−C/C−H component at 285 eV. The surface compositions, in atomic ratios, were determined by considering the integrated areas of the C1*s*, S2*p*, O1*s*, Sn3$d_{5/2}$, and In3$d_{5/2}$ core-level peaks and the respective manufacturer's sensitivity factors.

Supporting Information Available: Orientation analysis of the IR absorption data. This material is available free of charge via the Internet at http://pubs.acs.org.

LA052677B